THE EFFECT OF LOADING MODE ON THE STRUCTURAL RESPONSE OF HUMAN SPINE WITH UNCONTAINED OSTEOLYTIC DEFECT: A COMPUTATIONAL STUDY

Ron N. Alkalay, Ph.D[1]., Raymond Oschsenbein M.S.c[1], Timothy Harrigan, Ph.D[2]

[1]Orthopedic Biomechanics Laboratory, Beth Israel Deaconess Medical Center, and [2] Foster-Miller Inc., Waltham, MA.

Introduction

Cancer, second to only heart attack as the leading cause of death in the US, affects up to one-third of all cancer patients suffering from metastatic involvement of the spine. Osteolytic lesions greatly increase the risk of pathologic fracture of the vertebra. Previous studies demonstrated the risk of pathologic fracture to be dependent on tumor volume, its shape, bone density, involvement of the pedicles and activity level. However, the effects of osteolytic defect on the internal deformation of the affected vertebra and the transfer of loading both within the vertebra as well as with its adjacent vertebrae under functional loads, remains unclear.

Objectives

To investigate the effect of loading conditions on the internal deformation and correspondigly the stress /strain environment of a L2-L3 human spine segment with a simulated non-contained osteolytic defect.

Methods

Computer Tomographic Imaging

- An L2-L3 human cadaveric spinal unit was obtained fresh-frozen from a 65 year old donor through the Anatomic Gift Foundation (Maryland).
- The spine was mounted within a specialized computer controlled CT-compatible loading frame developed in the OBL (Fig. 1) and the assembly positioned in a 64 array helical CT scanner (Aquilion 64, Toshiba Medical, CA).
- *Intact Spine*: A reference image was obtained yielding a series of axial cross sections, 0.5 millimeter thick at 0.5 millimeter apart. The spine was exposed to compressive loading in three equal steps to a value of 750N with new set of CT images obtained for each load step (Fig. 2).
- *Osteolytic defect*: Under fluoroscopic control, a 50% non-contained defect was created within the top vertebral body using an expanding reamer (Fig. 2). The sequence of mechanical loading and acquisition of CT images was then repeated.

Figure 1 A pictorial representation of the CT compatible testing device. **A**: servo motor (SM 233, Parker Hannifin Co, CA), **B**: driving mechanism and **C:** loading platen, **D**: the specimen mounting ring, **E**: 6DOF load cell and **F**: Torlon™ rods.

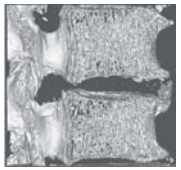

Figure 2. A midsagittal image obtained from the CT of the intact spine using the CT compatible testing device.

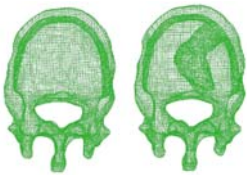

Figure 3. TrueGrid parametric mesh models of an intact vertebra, and with an uncontained defect created within the body.

Finite Element Model

- *Segmentation*: The CT volumes were reconstructed to yield axial slices, 0.2mm thick with in-plane resolution of (0.161^{-2})mm and the stack of axial images imported to MIMICS™ (10, Materialize Inc., Leuven, Belgium). For the intact and osteolytic defect spine image volumes, the vertebrae and disc were segmented, a surface model produced for each segmented volume, the polygonal surface optimized, and the volume exported as an .stl file.
- *Parametric Mesh Modeling*: Using shape-based templates in TrueGrid (XYZ Scientific Application Inc. Livermore, CA), developed in the OBL, parametric hexahedral mesh models with a resolution of 0.70-0.83mm per element were implemented for each vertebral and disc geometry (Fig 3). This high resolution offers a balance between the computational complexity of the model and the ability to model the mechanical response of the vertebra.
- *Allocation of Material Models*: The ability to model local variations in material properties of either cancellous or vertebral cortex for a specific specimen significantly determines the ability of the computational model to account for the mechanical behavior of vertebral segments under physiological loading scenarios. The parametric mesh models were re-imported into MIMICS 10 and density-based material models used to assign material properties for each element (Fig 4).
- *Assembly of computational model*: The density weighted mesh models were imported into ABAQUS (6.5.4, Simulia, RI), Fig 5. The vertebrae and disc were assembled to recreate the spine segment, spinal ligaments ((Facets, anterior and posterior longitudinal and spinous process added, (structures in purple color, Fig. 5)), with the intervertebral disc represented as a fiber reinforced disc model to more accurately simulate the collagen structures of the annulus. This process was repeated for the spine with the uncontained osteolytic defect within the upper vertebra (Fig. 5). Both the intact and defect models were subjected to either compressive (750N) or compressive + torsion (5Nm) monotonic loading.

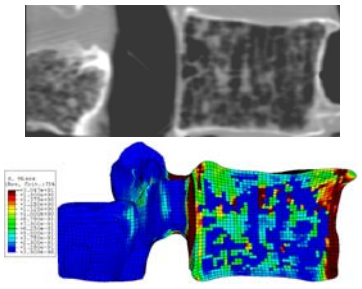

Figure 4. Illustrates a cross sectional CT image of the vertebra and corresponding stress distribution computed for the vertebra under compressive load demonstrating load sharing between the cortex and internal the trabecular bone

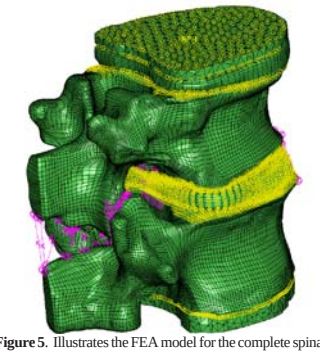

Figure 5. Illustrates the FEA model for the complete spinal segment. Purple line represent the ligaments. Yellow circles represent constraint conditions between the various structures.

Results

- **Compression loading:** Compared to the intact spine, the inclusion of the uncontained defect led to marked increase in compressive loading at the anterior portion of the cortex (70%, Fig. 6.A vs. 6.B) and at the medial lateral and posterior portion of the cortex (19%). Marked increase in shear stresses along both M-L(S32) and A-P (S12) plane can be observed at the posterior cortex near the defect, at the anterior cortex as well as at the pedicles (Fig 6.C vs. 6.D).
- **Addition of torque:** The addition of torsion loading (Fig. 7) resulted in the development of marked A-P shear stresses at the vertebral cortex as well as, marked changes in the compressive stress within both vertebrae (Fig 7A vs. 7B). Significantly, the addition of torque led to marked increase in shear stress at the vertebral cortex with the highest increase observed at the posterior vertebral cortex (P3, Fig 7.). Of note was a complete reversal in the sign for several of the stress indices (7.C).

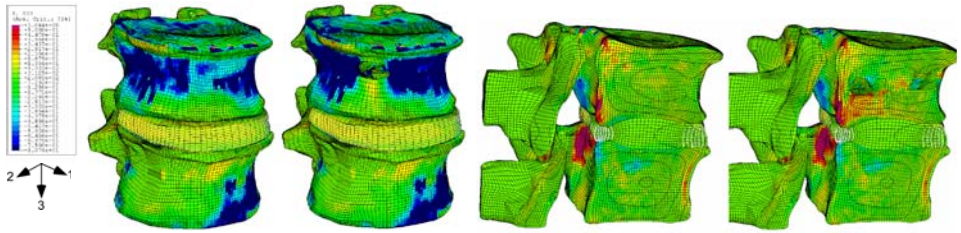

Figure 6. Illustrates the effect of 750N compression load on the compressive and shear stress distributions of the intact (A and C) and metastatic (B and D) spine.

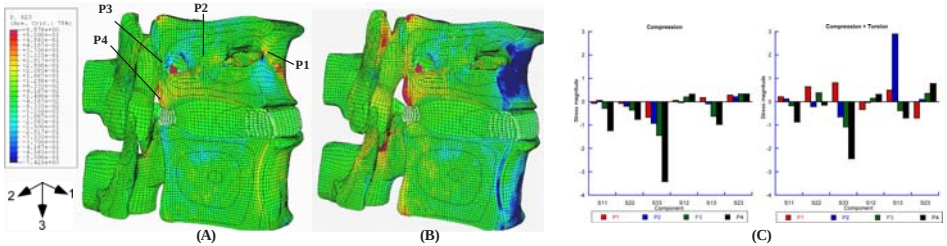

Figure 7. Comparison of the shear stress distributions (S23) within metastatic spine under 750N compressive load (A) and with the addition of 5 Nm torsional load (B) The effect of torsional loading on the change in stress components for selected locations at the cortex and within the defect is presented in Fig 7.C.

Discussion

This preliminary high-resolution computational study highlighted the effect of osteolytic defect and loading condition on the structural response of human lumbar spine. This provides a platform for studying fracture and failure processes involving metastatic tumors of the spine, and for addressing several clinical decisions that are relevant to care for patients with tumors of the spine. This work will inform decisions such as when to intervene and which of several available techniques and material choices are best for the type and size of defect seen. Since patients with metastatic spine tumors often have a poor prognosis, every day of comfortable function that can be provided is very valuable. This work is aimed at developing technology to provide that function.

The authors would like of thank the Robert Mathys Foundation, Bettlach, Switzerland for their kind support for this project